Simultaneous Anodic and Cathodic Formate Production in a Paired Electrolyzer by CO_2 Reduction and Glycerol Oxidation

João R. C. Junqueira,[a] Debanjan Das,[a] Ann Cathrin Brix,[a] Stefan Dieckhöfer,[a] Jonas Weidner,[a] Xin Wang,[a] Jialin Shi,[a] and Wolfgang Schuhmann*[a]

Electrochemical CO_2 conversion is a key technology to promote the production of carbon-containing molecules, alongside reducing CO_2 emissions leading to a closed carbon cycle economy. Over the past decade, the interest to develop selective and active electrochemical devices for electrochemical CO_2 reduction emerged. However, most reports employ oxygen evolution reaction as an anodic half-cell reaction causing the system to suffer from sluggish kinetics with no production of value-added chemicals. Therefore, this study reports a con-ceptualized paired electrolyzer for simultaneous anodic and cathodic formate production at high currents. To achieve this, CO_2 reduction was coupled with glycerol oxidation: a BiOBr-modified gas-diffusion cathode and a Ni_xB on Ni foam anode keep their selectivity for formate in the paired electrolyzer compared to the half-cell measurements. The paired reactor here reaches a combined Faradaic efficiency for formate of 141% (45% anode and 96% cathode) at a current density of 200 mA cm^{-2}.

Introduction

The electrochemical CO_2 reduction reaction (CO_2RR) is a promising strategy to produce chemical fuels and feedstock. Formate (HCO_2^-) was identified as an economically viable CO_2RR product.[1] Among others such as Sn-based catalysts,[2] Bi-derived materials were shown to be particularly suitable for CO_2 reduction to formate.[3–5] Bi-derived catalysts can be produced from non-toxic and abundant raw materials while displaying high activity[6] and stability.[7] Bismuth oxyhalides (BiOX) where X = I, Br, or Cl are generally layered 2D materials[5] and yield catalysts with a high surface area under reductive conditions.[4] The utilization of gas-diffusion electrodes (GDE) for the CO_2RR unlocks the possibility to perform this reaction without mass transport limitations.[8] Thus, reaching high current densities in alkaline electrolytes, alongside mitigating the parasitic hydrogen evolution (HER) reaction is possible.[9]

Usually, the CO_2RR is performed in a two-compartment cell, i.e., the cathode and the anode, where the reduction and oxidation reactions take place, respectively, which are separated by a membrane. In this case, the cathodic half-cell reaction is the CO_2RR and typically the anodic half-cell reaction is the oxygen evolution reaction (OER) as represented in Figure 1a. Besides O_2 not being a valuable industrial product, the OER in alkaline media suffers from sluggish kinetics and requires a large overpotential.[10,11] Coupling the CO_2RR with the OER ultimately leads to only half of the reactor being dedicated to the production of value-added products, thereby limiting the economic feasibility of such a device. Therefore, alternative anodic reactions, for example, the oxidation of alcohols or organic molecules, were coupled with CO_2RR to decrease the overall required cell voltage and increase the yield of valuable products.[10–13]

[a] Dr. J. R. C. Junqueira, Dr. D. Das, A. Cathrin Brix, Dr. S. Dieckhöfer, J. Weidner, X. Wang, Dr. J. Shi, Prof. Dr. W. Schuhmann
Analytical Chemistry – Center for Electrochemical Sciences (CES), Faculty of Chemistry and Biochemistry
Ruhr-Universität Bochum
Universitätsstraße 150, 44780 Bochum Department (Germany)
E-mail: wolfgang.schuhmann@ruhr-uni-bochum.de

Supporting information for this article is available on the WWW under https://doi.org/10.1002/cssc.202202349
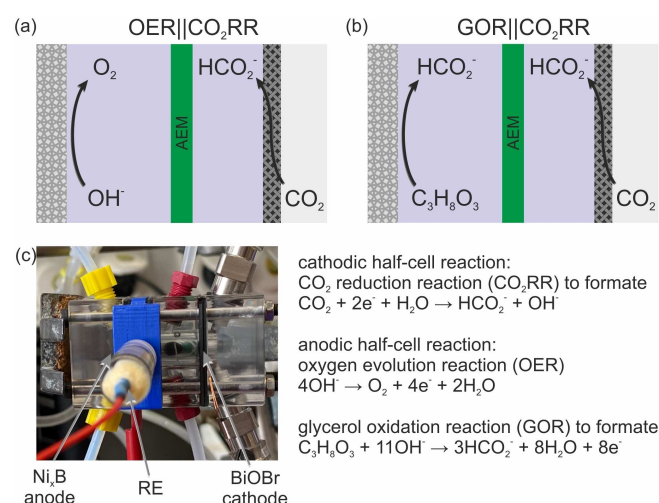
Figure 1. Schematic representation of an OER||CO_2RR reactor (a) and a GOR||CO_2RR paired electrolysis reactor (b), picture of the used paired electrolyzer (c).

cathodic half-cell reaction:
CO_2 reduction reaction (CO_2RR) to formate
$CO_2 + 2e^- + H_2O \rightarrow HCO_2^- + OH^-$

anodic half-cell reaction:
oxygen evolution reaction (OER)
$4OH^- \rightarrow O_2 + 4e^- + 2H_2O$

glycerol oxidation reaction (GOR) to formate
$C_3H_8O_3 + 11OH^- \rightarrow 3HCO_2^- + 8H_2O + 8e^-$

ChemSusChem

Research Article
doi.org/10.1002/cssc.202202349

Chemistry Europe
European Chemical
Societies Publishing

The simultaneous production of valuable products from both anodic and cathodic half-cell reactions in a two-compartment reactor separated by a membrane is referred to as a paired electrolyzer.[12] Few reports showed results of a paired electrolyzer performing CO_2RR on the cathode side combined with the methanol,[14,15] ethanol,[16] octylamine,[17] hydroxymethylfurfural (HMF),[18] PET,[19] glycerol,[11,20,21] or formaldehyde[22] oxidation as the anodic half-cell reaction. These studies showed that a paired electrolyzer can lower the cell voltage with concomitant increased production of valuable products. Yet, these studies have not shown the performance of a paired electrolyzer at current densities higher than 100 mA cm^{-2}, thus limiting their potential practical implementation. The combination of the CO_2RR and an alternative anode reaction for the simultaneous production of formate is considered for enhanced formate production.[23]

Glycerol is the major side product of biodiesel production and its oxidation results in a variety of valuable chemicals.[24,25] Additionally, the glycerol oxidation reaction (GOR) displays low anodic overpotentials and a high yield of formate as the major product.[24,26] Among Ni-based materials, Ni-boride (Ni$_x$B) catalysts were shown as active catalysts for the GOR to formate.[26,27]

This work describes a further step in the development process of a paired electrolyzer capable of concurrently producing formate on both cathode and anode. A paired electrolyzer was developed, combining BiOBr on a GDE as an electrocatalyst for the CO_2RR and Ni$_x$B as an electrocatalyst for the GOR for simultaneous formate production at high current densities (Figure 1b).

Results and Discussion

BiOBr was synthesized via a solvothermal method.[28] Scanning electron microscopy (SEM) micrographs of the particles loaded on the GDE were obtained before and after electrolysis (Figure 2a and b). Pristine BiOBr was composed of nanosheets assembled into a flower-like structure. After electrolysis, the original shape changes to broken layered particles. X-ray photoelectron spectroscopy (XPS) measurements were conducted to evaluate the changes in the chemical nature of the catalyst surface during electrolysis. The Bi 4f region spectrum of the as-synthesized powder was deconvoluted into one 4f$_{5/2}$ and one 4f$_{7/2}$ component at 164.4 and 159.1 eV, respectively, suggesting the presence of Bi^{3+} species (Figure S1).[29,30] Additionally, the fit of the O 1s region reveals the presence of distinct Bi^{3+} surface species, as represented by the Bi–O and Bi(OH)$_3$ binding energies at 530.0 and 531.2 eV, respectively.[30] Finally, the presence of at least two different bromide species was suggested by the peak fit of the Br 3d region, considering that two Br 3d$_{5/2}$ components at 68.2 and 69.2 eV were necessary to obtain a reasonable fit.[31] After electrolysis, the chemical surface composition of the catalyst changed (Figure S1). The Bi 4f peak shifted to lower binding energies, suggesting a higher electron density at Bi surface sites. This is supported by the increased contribution of the Bi(OH)$_3$ in the O 1s region. No Br was detected on the catalyst surface after electrolysis. This finding emphasizes that the pristine BiOBr is a pre-catalyst, that undergoes halide leaching under the reductive condition to yield the active material.[4]
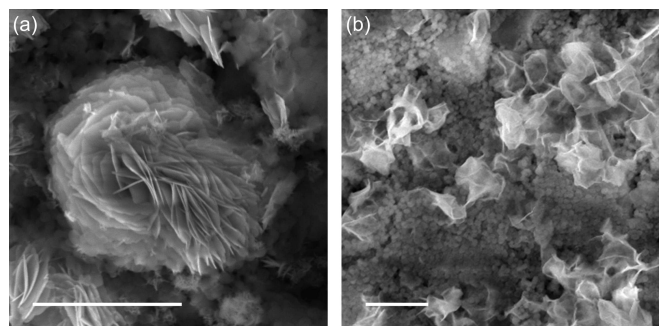
The Ni$_x$B anode was prepared following a solid-state thermal procedure published previously.[26] Briefly, boron powder was dispersed on Ni foam, which was later inserted into a tube furnace at 1000 °C for 5 h in an Ar atmosphere. The SEM micrographs indicate that during preparation, the initially smooth surface changed to a highly decorated surface with sharp particles (Figure 3). The XPS surface analysis of the formed Ni$_x$B exhibit in addition to a dominant Ni(OH)$_2$ multiplet structure the Ni 2p$_{3/2}$ peak, which highlights the presence of multiple components below 853.7 eV (Figure S2). These peaks correspond to reduced surface species compared to the commonly stable +II state. Besides partially oxidized Ni and Ni^0 with main components at 853.4 and 852.6 eV, respectively, a low binding energy component at 851.9 eV suggested the

Figure 2. SEM micrographs of BiOBr particles before (a) and after (b) electrolysis, the scale bar represents 3 μm.
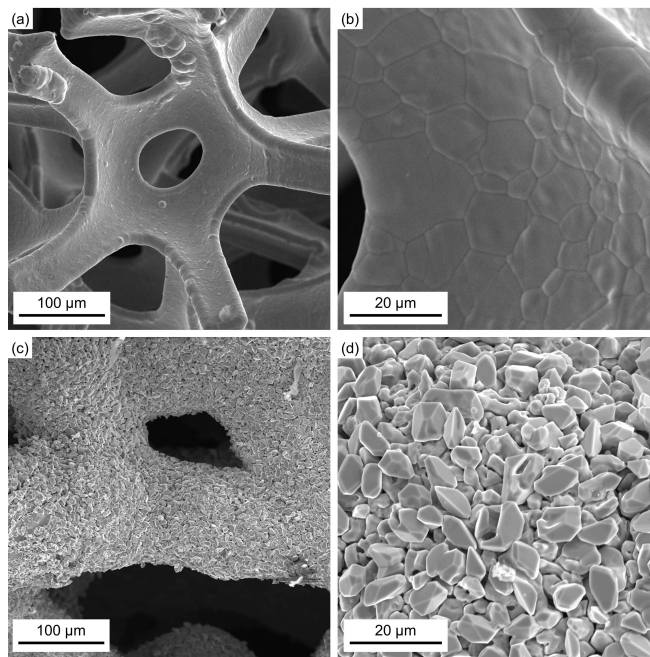
Figure 3. SEM micrographs of Ni foam (a and b) and Ni$_x$B (c and d) at different magnifications.

ChemSusChem

Research Article
doi.org/10.1002/cssc.202202349

Chemistry Europe
European Chemical
Societies Publishing

formation of Ni-boride species.[32] Such positive binding energy shift of metal boride species (relative to the metallic state) has been previously observed and explained by a partial charge transfer between metal and boron.[33,34] The presence of a Ni–B interaction was further supported by the B 1s region, where two major components in the peak fit model at 192.7 eV and 187.8 eV were assigned to Bi_2O_3 and boride species,.[33] To evaluate the Ni-to-B ratio, inductively coupled plasma mass spectrometry (ICP-MS) was used. The results show a Ni-to-B molar ratio of 3:1, indicating the formation of Ni_3B particles. After electrolysis, the Ni-to-B molar ratio increased to 14.4:1, indicating B leaching under oxidation conditions (Table S1). SEM micrographs after electrolysis show the loss of the initially sharp particles on the Ni foam surface (Figure S3). XPS analysis of the sample after electrolysis reveals the loss of Ni^0 and Ni-boride contributions to the signal envelope rendering oxidized Ni in $Ni(OH)_2$ as the remaining surface species. Interestingly, the B 1s region indicated a transformation of boride into an oxidized form rather than a complete loss of boron surface species due to leaching. These findings suggest an oxidation of the anode during electrolysis.

All measurements were performed in a two-compartment flow-through reactor (Figure 1c) separated by a Nafion 117 membrane with a constant flow of the electrolyte (Figure S4a and b). To record the potential of the working electrode (WE) and counter electrode (CE), a three-electrode system was used with a double-junction $Ag|AgCl|KCl$ (3 mol L^{-1}) reference electrode inserted in the working electrode compartment. Galvanostatic measurements were performed by applying constant current densities of 25, 50, 100, 150, and 200 mA cm^{-2}, respectively, for 14.9 min, followed by galvanostatic electrochemical impedance spectroscopy (GEIS) at each current density value (Figure S5). During chronopotentiometry, both the WE and CE potentials were recorded. The results are presented in current density (j_{geo}) calculated from the geometric surface area of 0.95 cm^2. The electrolyte, 1 mol L^{-1} KOH, was circulated at a constant flow rate of 19 mL min^{-1}. For the GOR, 1 mol L^{-1} glycerol was added to the anolyte.

Initially, the performance of the cathode and anode was evaluated in half-cell reactions making the respective counter electrode not limiting. The CO_2RR selectivity of BiOBr was evaluated in a flow-through cell with the OER as an anode reaction. The results show high selectivity of the cathode material for formate production with a Faradaic efficiency (FE) of around 92% at current densities between 25 and 200 mA cm^{-2}. An additional minor formation of CO and H_2 was detected with Faraday efficiencies of about 3 and 1%, respectively (Figures 4a and S5a).

These results confirm the selectivity of the BiOBr catalyst for formate production in a broad range of applied current densities and a minor competitive contribution by the HER. In the case of the GOR, a predominant selectivity for the formation of formate was obtained with the highest value of ~71% at 25 mA cm^{-2} (Figures 4b and S5b). Other compounds, such as oxalate ($C_2O_4^{2-}$), tartronate ($C_3H_2O_5^{2-}$), glycerate ($C_3H_5O_4^-$), glycolate ($C_2H_3O_3^-$), lactate ($C_2H_5O_3^-$) and acetate ($C_2H_3O_2^-$), were also detected with lower selectivity.
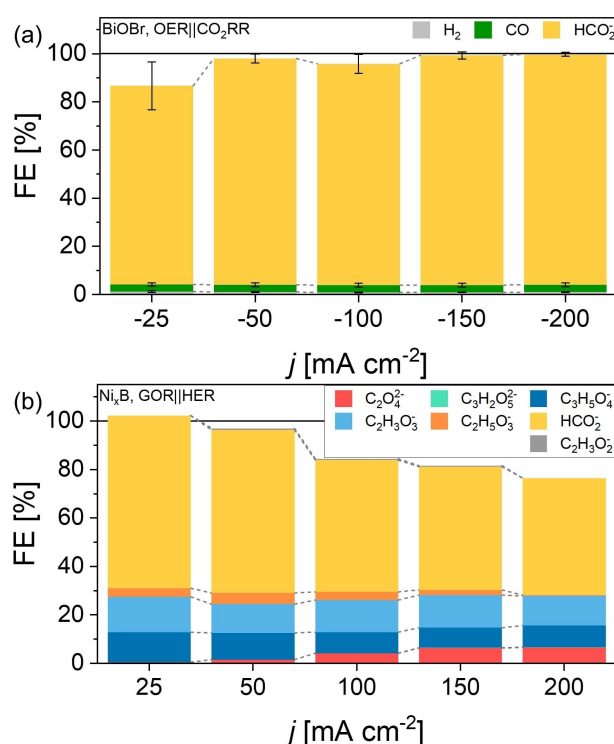
Figure 4. Product distribution of half-cell measurements for the BiOBr cathode (a) and the Ni_xB anode (b). CO_2 flow: 12 mL min^{-1}; 1 mol L^{-1} KOH, electrolyte flow: 19 mL min^{-1}. GOR measurement in the presence of 1 mol L^{-1} glycerol. Values from Tables S2 and S3.

Once both the Ni_xB anode and the BiOBr cathode were individually evaluated in half-cell experiments and high selectivities for formate production were determined, the performance of concerted production of formate in a paired electrolysis was evaluated. For this purpose, a two-compartment model electrolyzer separated by a Nafion 117 membrane was used (Figures 1c and S4c). However, the combination of two half-cell reactions is challenging, especially if the kinetics are very different. In the paired electrolyzer the anode and cathode were connected to a three-electrode system, in which the anode, Ni_xB on Ni-foam, a double-junction $Ag|AgCl|KCl$ (3 mol L^{-1}) and the cathode, BiOBr on GDE, represented the WE, RE, and CE, respectively. The half-cell experiment showed that the Ni_xB selectivity for the GOR to formate was potential dependent.[26] Therefore, to keep the anode potential as small as possible during the galvanostatic measurements, the RE-to-anode distance was kept as minimal as possible (Figure S4d) and the size of the anode was increased. Since the BiOBr GDE is the not-limiting electrode and the selectivity is less current dependent, in the paired electrolyzer the BiOBr GDE was connected as the counter electrode and hence polarized to high cathodic potentials (Figure S6a).

Figures 5 and S6 display the results of the cathode and anode performance during paired electrolysis. The product distributions of both the anode and cathode are similar to the half-cell measurements. The formate selectivity on the cathodic side was ~96% and on the anodic side ~54%. The simultaneous formate production added up to an overall Faraday

ChemSusChem

Research Article
doi.org/10.1002/cssc.202202349

Chemistry
Europe
European Chemical
Societies Publishing
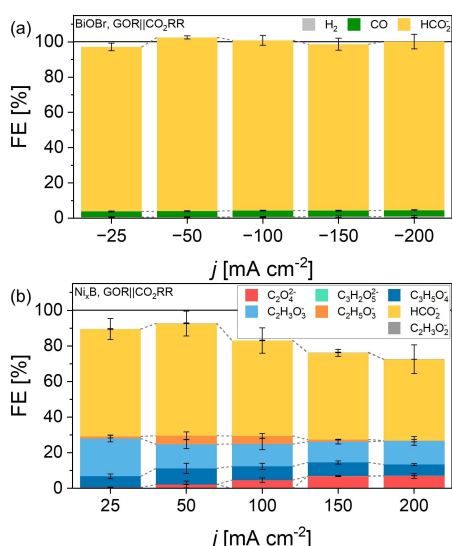
Figure 5. Product distribution of paired electrolyzer for a BiOBr-GDE cathode (a) and Ni_xB anode (b). CO_2 flow: 12 mL min^{-1}; 1 mol L^{-1} KOH; electrolyte flow: 19 mL min^{-1}. GOR measurements in the presence of 1 mol L^{-1} glycerol. Average and standard deviations from 3 independent experiments. Values from Tables S4 and S5.

Figure 6. Obtained formate selectivity using the paired electrolyzer for the BiOBr-GDE cathode (blue) and Ni_xB anode (yellow) FE at different current densities for 2.5 h (b). Values from Tables S6 and S7. CO_2 flow 12 mL min^{-1} 1 mol L^{-1} KOH, electrolyte flow 19 mL min^{-1}. GOR experiment in the presence of 1 mol L^{-1} glycerol.

efficiency of 161% (63% anode and 98% cathode) at 50 mA cm^{-2} and 141% (45% anode and 96% cathode) at 200 mA cm^{-2} (Figure S7). The paired electrolyzer reached a total formate production of 4.6 mmol h^{-1} (Figure S9a) and after electrolysis, formate concentrations of 95 mmol L^{-1} in the anolyte and 276.2 mmol L^{-1} in the catholyte were measured (Figure S9b).

In contrast to recent works reporting simultaneous production of formate in paired electrolyzers,[14,15,19,20,22] our proposed system exhibits selectivity for formate of ~141% (45% anode and 96% cathode) at a current density of 200 mA cm^{-2}. Hence, the present paired electrolysis approach provides substantially increased formate production, reaching up to 282.8 mA cm^{-2} (Figure S10 and Table S8).

After testing the paired electrolyzer at different current densities, a further constant current density experiment was performed. The results show a total FE for formate of ~153% (~57% anode and ~96% cathode) at 100 mA cm^{-2} for 2 h (Figures 6 and S8, and Tables S6 and S7).

To determine the efficiency of the paired electrolyzer in relation to the half-cell configuration, the ratio between energy output from the formate production and the energy demanded by the different electrolyzer configurations was calculated. The results show that the combination of CO_2RR with GOR increases the reactor energy efficiency. The GOR||CO_2RR is 41% more efficient when compared to the OER||CO_2RR, and 203% more efficient than HER||GOR at 200 mA cm^{-2}. Additionally, a CO_2 balance estimation was performed. The results indicate that the difference between the CO_2 consumption on the cathode for the exclusive formate production and the maximal possible release of CO_2 by the complete oxidation of glycerol equals circa -2.9×10^{-3} mol h^{-1} or -7.2×10^{-5} m^3 h^{-1} of CO_2 at
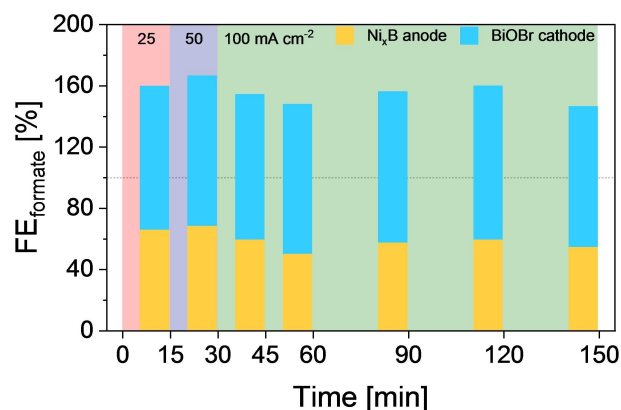
200 mA cm^{-2} (details of these calculations can be found in the Supporting Information). These results show that the paired electrolyzer has a higher energy efficiency when compared to the half-cell measurements, and the process consumes more CO_2 than it releases.

Conclusion

A GDE-based BiOBr cathode to selectively convert CO_2 to formate with an average FE of ~92% and a Ni_xB anode for the glycerol oxidation to formate with an average FE of ~58% up to 200 mA cm^{-2} in half-cell measurements were combined for simultaneous formate generation in a paired electrolyzer. Paired electrolysis measurements reached a total FE of ~141% (45% anode and 96% cathode) at 200 mA cm^{-2}. Moreover, the individual selectivity of the electrodes when measured in the paired electrolyzer configuration was similar to that of the half-cell measurements. This study demonstrates the utilization of a paired electrolyzer for the simultaneous production of formate at previously not achieved current densities as a suitable strategy for increasing the production of valuable chemicals in conjunction with electrochemical CO_2RR.

Experimental Section

Preparation of Ni_xB as anode

Boron powder (Merck) was dispersed on pre-cut Ni foam (3 mm thick, Goodfellow). A circular piece of 10 mm in diameter and a square of 1.5 cm × 1.5 cm were placed inside a quartz boat, which was later inserted into a tube furnace. The sample was heated at 10 °C min^{-1} to 1000 °C which was kept for 5 h in an Ar atmosphere. After the thermal synthesis, the electrodes were rinsed with water to remove the remaining boron powder and used for the electrolysis.

Preparation of a BiOBr-GDE as cathode

$0.1\,\mathrm{mol\,L^{-1}}$ $Bi(NO_3)_3 \cdot 5\,H_2O$ (Merck) was dissolved in 25 mL of $1.25\,\mathrm{mol\,L^{-1}}$ glacial acetic acid (Merck) and stirred for 30 min. Then, $2\,\mathrm{mol\,L^{-1}}$ KBr (Merck) solution was added dropwise to the above solution, followed by the addition of $1\,\mathrm{mol\,L^{-1}}$ KOH (VWR) for adjusting the solution pH to 6.5. The yellowish-white suspension was stirred for an additional 30 min before transferring it to a 50 mL Teflon-lined autoclave followed by hydrothermal treatment at 160 °C for 1 h. The final product was collected by centrifugation, repetitively washed with deionized water, and once with ethanol. Finally, it was dried at 70 °C overnight. After the catalyst synthesis, suspensions containing $1\,\mathrm{mg\,mL^{-1}}$ of the BiOBr particles and $0.5\,\mathrm{mg\,mL^{-1}}$ PTFE 1 μm particles (Sigma) were prepared in ethanol (VWR) and sonicated for 15 min. The suspension was drop-casted on a gas-diffusion layer (H23C2, Freudenberg), resulting in a $1\,\mathrm{mg_{BiOBr}\,cm^{-2}}$ GDE.

Materials characterizations

Scanning electron micrographs were recorded using a Quanta 3D ESEM (FEI) operated at 20.0 kV in high vacuum mode. X-ray photoelectron spectroscopy (XPS) measurements were carried out using an AXIS Nova spectrometer equipped with a monochromatic Al K_α X-ray source (1487 eV, 15 mA emission current). Throughout the XPS analysis, a constant chamber pressure of around 10^{-8} Torr was maintained. XPS survey spectra were recorded in the fixed transmission mode (20 eV pass energy) while achieving charge compensation by means of an electron flood gun. Calibration of the binding energy scale was conducted by assigning the C–C component of the C 1s spectrum to a value of 284.8 eV. Inductively coupled plasma mass spectrometry (ICP-MS) was performed with an iCAP RQ (Thermo Fisher) instrument in KED mode (collision cell mode with helium as collision gas). The elements were calibrated with standards between 0 and 100 ppb. Prior to the measurement, around 10 mg of the sample were solubilized in 300 μL of 2% HNO_3 solution (36%, Roth) and digested at 90 °C for 15 min.

Electrochemical measurements

All electrochemical measurements were performed using a three-electrode system controlled by a VMP-3 potentiostat (BioLogic). The reference electrode was a homemade Ag|AgCl|KCl $(3\,\mathrm{mol\,L^{-1}})$ with a double junction filled with $1\,\mathrm{mol\,L^{-1}}$ KOH. Initially, a galvanostatic linear polarization curve (GLPC) from 0 to $25\,\mathrm{mA\,cm^{-2}}$ at $0.1\,\mathrm{mA\,s^{-1}}$ was recorded followed by chronopotentiometries at 25, 50, 100, 150, and $200\,\mathrm{mA\,cm^{-2}}$ for 14.88 min and finally a galvanostatic electrochemical impedance spectroscopy from 100 kHz to 2 Hz with the amplitude current at 10% of the applied current. The electrolyte reservoirs were filled with 10 mL of $1\,\mathrm{mol\,L^{-1}}$ KOH (VWR) (pH 13.9) purified with a Chelex 100 column and in the case of the anode electrolyte, an additional 1 mL of glycerol solution (~86.5% in water Merck) was added. For the whole measurement duration, the electrolyte was recirculated at $19\,\mathrm{mL\,min^{-1}}$ with a Perimax 12 peristaltic pump (Spetec). The catholyte was constantly purged with $16\,\mathrm{mL\,min^{-1}}$ N_2 and a CO_2 flow of $12\,\mathrm{mL\,min^{-1}}$ was applied. Both gas flows were controlled with mass flow controllers (GFC-171, AALBORG).

The flow reactor was fabricated from poly(methyl methacrylate) (PMMA) by the fine mechanic workshop of the faculty of chemistry and biochemistry of the Ruhr University Bochum. The RE compartment was 3D printed with Apollo-X filament. The anode and cathode compartments were separated by a Nafion 117 membrane (Merck). The geometric area of BiOBr on the GDE which is exposed to the electrolyte was $0.95\,\mathrm{cm^2}$.

All potentials are reported versus the reversible hydrogen electrode (RHE) and were calculated following Equation (1).

$$E_{RHE} = E_{Ag|AgCl|KCl(3\,mol\,L^{-1})} + 0.210 + (0.059^* pH) \tag{1}$$

Products analysis

Gaseous products were analyzed with an MG#1 gas-chromatograph (GC, SRI Instruments) equipped with a 3 m HayeSep D column, a thermo-conductive detector (TCD), and a flame ionization detector methanizer (FIDmeth). The TCD was used to quantify the amount of H_2 while CO was determined using the FIDmeth. The carrier gas was N_2 (N95, AirLiquide) and the column was kept at a constant temperature of 75 °C. For comprehensive analyzes of the gaseous products, two GC injections were performed each 7.5 min per applied current. The first injection was from the catholyte head-space and the second injection was from the products in the CO_2 stream. The FE of the gaseous products was calculated using Equation (2).

$$FE_n = \frac{z_n \times x_n \times f \times F}{i_t \times 10^6 \times V_m} \times 100\% \tag{2}$$

FE_n is the faradaic efficiency for product n in %, z_n is the product-specific number of transferred electrons, x_n is the product-specific concentration detected by the GC in ppm, f is the gas flow in $L\,s^{-1}$, F is the Faraday constant ($96485\,C\,mol^{-1}$), i_t is the total current at the injection time in A, 10^6 is the conversion factor of ppm to vol% and V_m is the molar volume of an ideal gas at 25 °C ($24.5\,L\,mol^{-1}$).

Liquid products were analyzed with high-performance liquid chromatography (HPLC). A Dionex ICS-5000 (ThermoFisher) equipped with an ion-exclusion column Aminex HPX-87H (Bio-Rad), a diode array detector (using the wavelength of 220 nm), and a refractive index (RI) detector (RefractoMax520) was used. Formic acid was analyzed with the UV detector and the other molecules with the RI detector. The eluent was $4\,\mathrm{mmol\,L^{-1}}$ H_2SO_4 at a flow rate of $0.6\,\mathrm{mL\,min^{-1}}$ and the column temperature was kept constant at 70 °C. After each current step, a 540 μL aliquot was collected from the anolyte and catholyte reservoirs. Prior to HPLC injections, the samples were acidified by mixing 440 μL of the collected aliquots with 110 μL of $2.5\,\mathrm{mol\,L^{-1}}$ H_2SO_4. The FE of the liquid products was calculated using Equations (3) to (5).

$$mr_{n-b} = c_{n-b} \times f_{dil} \times V_{reactor_b} \tag{3}$$

$$pm_{n-s1} = mr_{n-s1} - mr_{n-b} \tag{4}$$

$$FE_n \frac{F \times z_n \times pm_{n-s1}}{sf_n \times \int i} \times 100\% \tag{5}$$

mr_{n-b} is the number of moles for product n in the reactor for aliquot b, c_{n-b} is the product-specific concentration detected by HPLC in $mol\,L^{-1}$, f_{dil} is the dilution factor from the sample acidification (1.25) and $V_{reactor}$ is the volume before the aliquot b was collected in L. pm_{n-s1} is the produced moles of product n for aliquot s1 and mr_{n-s1} is the number of moles of product n in the reactor for aliquot s1. FE_n is the product-specific faradaic efficiency in %, F is the Faraday constant ($96485\,C\,mol^{-1}$), z_n is the product-specific number of transferred electrons, sf_n is the product-specific stoichiometric factor (see Eqs. (S1) to (S10)),[24] and the current i was integrated over the accumulation period.

Conflict of Interest

The authors declare no conflict of interest.

Data Availability Statement

The data that support the findings of this study are available from the corresponding author upon reasonable request.

[1] S. Nitopi, E. Bertheussen, S. B. Scott, X. Liu, A. K. Engstfeld, S. Horch, B. Seger, I. E. L. Stephens, K. Chan, C. Hahn, J. K. Nørskov, T. F. Jaramillo, I. Chorkendorff, *Chem. Rev.* **2019**, *119*, 7610.

[2] a) A. Löwe, M. Schmidt, F. Bienen, D. Kopljar, N. Wagner, E. Klemm, *ACS Sustainable Chem. Eng.* **2021**, *9*, 4213; b) K. Ye, Z. Zhou, J. Shao, L. Lin, D. Gao, N. Ta, R. Si, G. Wang, X. Bao, *Angew. Chem. Int. Ed.* **2020**, *59*, 4814.

[3] a) G. Díaz-Sainz, M. Alvarez-Guerra, J. Solla-Gullón, L. García-Cruz, V. Montiel, A. Irabien, *J. CO2 Util.* **2019**, *34*, 12; b) K. Fan, Y. Jia, Y. Ji, P. Kuang, B. Zhu, X. Liu, J. Yu, *ACS Catal.* **2020**, *10*, 358; c) X. Wang, W. He, J. Shi, J. R. C. Junqueira, J. Zhang, S. Dieckhöfer, S. Seisel, D. Das, W. Schuhmann, *Chem. Asian J.* **2023**, *18*, e202201165.

[4] F. P. García de Arquer, O. S. Bushuyev, P. de Luna, C.-T. Dinh, A. Seifitokaldani, M. I. Saidaminov, C.-S. Tan, N. Li Quan, A. Proppe, M. G. Kibria, S. O. Kelley, D. Sinton, E. H. Sargent, *Adv. Mater.* **2018**, *30*, e1802858.

[5] J. Di, J. Xia, H. Li, S. Guo, S. Dai, *Nano Energy* **2017**, *41*, 172.

[6] a) T. Fan, W. Ma, M. Xie, H. Liu, J. Zhang, S. Yang, P. Huang, Y. Dong, Z. Chen, X. Yi, *Cell Rep. Phys. Sci.* **2021**, *2*, 100353; b) S. He, F. Ni, Y. Ji, L. Wang, Y. Wen, H. Bai, G. Liu, Y. Zhang, Y. Li, B. Zhang, H. Peng, *Angew. Chem. Int. Ed.* **2018**, *57*, 16114; c) Z. Wang, X. Zu, X. Li, L. Li, Y. Wu, S. Wang, P. Ling, Y. Zhao, Y. Sun, Y. Xie, *Nano Res.* **2022**, *15*, 6999.

[7] a) J. Lee, H. Liu, Y. Chen, W. Li, *ACS Appl. Mater. Interfaces* **2022**, *14*, 14210; b) J. Duan, T. Liu, Y. Zhao, R. Yang, Y. Zhao, W. Wang, Y. Liu, H. Li, Y. Li, T. Zhai, *Nat. Commun.* **2022**, *13*, 2039; c) M. Zhang, W. Wei, S. Zhou, D.-D. Ma, A. Cao, X.-T. Wu, Q.-L. Zhu, *Energy Environ. Sci.* **2021**, *14*, 4998.

[8] T. Burdyny, W. A. Smith, *Energy Environ. Sci.* **2019**, *12*, 1442.

[9] J. R. C. Junqueira, P. B. O'Mara, P. Wilde, S. Dieckhöfer, T. M. Benedetti, C. Andronescu, R. D. Tilley, J. J. Gooding, W. Schuhmann, *ChemElectroChem* **2021**, *8*, 4848.

[10] Á. Vass, A. Kormányos, Z. Kószó, B. Endrődi, C. Janáky, *ACS Catal.* **2022**, *12*, 1037.

[11] S. Verma, S. Lu, P. J. A. Kenis, *Nat. Energy* **2019**, *4*, 466.

[12] N. P. Martínez, M. Isaacs, K. K. Nanda, *New J. Chem.* **2020**, *44*, 5617.

[13] J. Na, B. Seo, J. Kim, C. W. Lee, H. Lee, Y. J. Hwang, B. K. Min, D. K. Lee, H.-S. Oh, U. Lee, *Nat. Commun.* **2019**, *10*, 5193.

[14] C. Cao, D.-D. Ma, J. Jia, Q. Xu, X.-T. Wu, Q.-L. Zhu, *Adv. Mater.* **2021**, *33*, e2008631.

[15] X. Wei, Y. Li, L. Chen, J. Shi, *Angew. Chem. Int. Ed.* **2021**, *60*, 3148.

[16] M. Bevilacqua, J. Filippi, A. Lavacchi, A. Marchionni, H. A. Miller, W. Oberhauser, E. Vesselli, F. Vizza, *Energy Technol.* **2014**, *2*, 522.

[17] Y. Liang, W. Zhou, Y. Shi, C. Liu, B. Zhang, *Sci. Bull.* **2020**, *65*, 1547.

[18] a) J. Bi, Q. Zhu, W. Guo, P. Li, S. Jia, J. Liu, J. Ma, J. Zhang, Z. Liu, B. Han, *ACS Sustainable Chem. Eng.* **2022**, *10*, 8043; b) S. Choi, M. Balamurugan, K.-G. Lee, K. H. Cho, S. Park, H. Seo, K. T. Nam, *J. Phys. Chem. Lett.* **2020**, *11*, 2941.

[19] J. Wang, X. Li, M. Wang, T. Zhang, X. Chai, J. Lu, T. Wang, Y. Zhao, D. Ma, *ACS Catal.* **2022**, *12*, 6722.

[20] Y. Pei, Z. Pi, H. Zhong, J. Cheng, F. Jin, *J. Mater. Chem. A* **2022**, *10*, 1309.

[21] M. S. E. Houache, R. Safari, U. O. Nwabara, T. Rafaïdeen, G. A. Botton, P. J. A. Kenis, S. Baranton, C. Coutanceau, E. A. Baranova, *ACS Appl. Energ. Mater.* **2020**, *3*, 8725.

[22] M. Li, T. Wang, W. Zhao, S. Wang, Y. Zou, *Nano-Micro Lett.* **2022**, *14*, 211.

[23] R. Li, K. Xiang, Z. Peng, Y. Zou, S. Wang, *Adv. Energy Mater.* **2021**, *11*, 2102292.

[24] X. Han, H. Sheng, C. Yu, T. W. Walker, G. W. Huber, J. Qiu, S. Jin, *ACS Catal.* **2020**, *10*, 6741.

[25] P. F. F. Amaral, T. F. Ferreira, G. C. Fontes, M. A. Z. Coelho, *Food Bioprod. Process.* **2009**, *87*, 179.

[26] A. C. Brix, D. M. Morales, M. Braun, D. Jambrec, J. R. C. Junqueira, S. Cychy, S. Seisel, J. Masa, M. Muhler, C. Andronescu, W. Schuhmann, *ChemElectroChem* **2021**, *8*, 2336.

[27] D. M. Morales, D. Jambrec, M. A. Kazakova, M. Braun, N. Sikdar, A. Koul, A. C. Brix, S. Seisel, C. Andronescu, W. Schuhmann, *ACS Catal.* **2022**, *12*, 982.

[28] N. Han, Y. Wang, H. Yang, J. Deng, J. Wu, Y. Li, Y. Li, *Nat. Commun.* **2018**, *9*, 1320.

[29] Z. Zhang, M. Chi, G. M. Veith, P. Zhang, D. A. Lutterman, J. Rosenthal, S. H. Overbury, S. Dai, H. Zhu, *ACS Catal.* **2016**, *6*, 6255.

[30] B. V. Crist, *J. Electron Spectrosc.* **2021**, *248*, 147046.

[31] I. Berlanga, *Biomol. Eng.* **2019**, *9*, 352.

[32] N. Wang, A. Xu, P. Ou, S.-F. Hung, A. Ozden, Y.-R. Lu, J. Abed, Z. Wang, Y. Yan, M.-J. Sun, Y. Xia, M. Han, J. Han, K. Yao, F.-Y. Wu, P.-H. Chen, A. Vomiero, A. Seifitokaldani, X. Sun, D. Sinton, Y. Liu, E. H. Sargent, H. Liang, *Nat. Commun.* **2021**, *12*, 6089.

[33] W. Hong, S. Sun, Y. Kong, Y. Hu, G. Chen, *J. Mater. Chem. A* **2020**, *8*, 7360.

[34] J. Masa, P. Weide, D. Peeters, I. Sinev, W. Xia, Z. Sun, C. Somsen, M. Muhler, W. Schuhmann, *Adv. Energy Mater.* **2016**, *6*, 1502313.

RESEARCH ARTICLE

A couple made in?: A conceptualized paired electrolyzer is proposed for the simultaneous anodic and cathodic formate production coupling the CO_2 reduction and the glycerol oxidation. A BiOBr-modified gas-diffusion cathode and a Ni_xB on Ni foam anode showed a combined Faradaic efficiency for formate of 141 % (45 % anode and 96 % cathode) at a current density of 200 mA cm^{-2}.
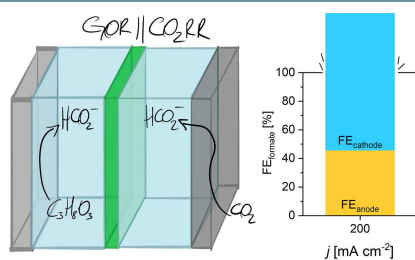
Dr. J. R. C. Junqueira, Dr. D. Das, A. Cathrin Brix, Dr. S. Dieckhöfer, J. Weidner, X. Wang, Dr. J. Shi, Prof. Dr. W. Schuhmann*

1 – 7

Simultaneous Anodic and Cathodic Formate Production in a Paired Electrolyzer by CO₂ Reduction and Glycerol Oxidation